## **Materials Horizons**



### COMMUNICATION

View Article Online



Double emulsion microencapsulation of ionic liquids for carbon capture†

Nicholas C. Starvaggi, Da Luma Al-Mahbobi, Db Muhammad Zeeshan, Dc Eliandreina Cruz Barrios, 🏴 Burcu Gurkan 📭 and Emily B. Pentzer 🕩 \*ab

Cite this: DOI: 10.1039/d4mh00796d

Received 21st June 2024 Accepted 13th September 2024

DOI: 10.1039/d4mh00796d

rsc.li/materials-horizons

Microencapsulation of pristine core liquids in polymer shells has

critical applications in thermal energy storage and management, targeted drug delivery, and carbon capture, among others. Herein, we report a novel encapsulation approach based on a double emulsion soft-template to produce microcapsules comprised of an ionic liquid (IL) core in a degradable polymer shell. We demonstrate the production of [IL-in-oil<sub>1</sub>]-in-oil<sub>2</sub> (IL/O<sub>1</sub>/O<sub>2</sub>) double emulsions, in which the oil interphase (O1) contains a CO2-derived polycarbonate bearing vinyl pendant groups, tetrathiol small molecule crosslinker, and photoinitiator; upon irradiation of the double emulsion under low shear, thiol-ene crosslinking of the loaded species results in the formation of a robust shell around the pure IL droplets. The coreshell structures have enhanced physisorption for CO2 uptake compared to the bulk IL, which is consistent with the combined capacity of the IL/shell alone and demonstrates more rapid uptake due to an enhanced gas-liquid interface. This approach to microencapsulation of functional liquids offers researchers a distinct route to fabricate composite architectures with a pristine core for applications in separations, transport of cargo, and gas uptake.

#### Introduction

Ionic liquids (ILs) describe a family of primarily organic-based salts with melting temperatures below 100 °C. 1-3 These compounds demonstrate several favorable properties, including enhanced ionic conductivity, 4,5 excellent thermal and chemical stability, 6,7 and negligible vapor pressures;8,9 consequently, their implementation as "greener" solvents in extractions, 10,11 separations, 12,13 and CO2 capture14,15 has garnered widespread interest. For example, high

#### New concepts

We report an innovative microencapsulation strategy for ionic liquids (ILs) based on an [IL-in-oil<sub>1</sub>]-in-oil<sub>2</sub> (IL/O<sub>1</sub>/O<sub>2</sub>) double emulsion soft-template. While double emulsions have been previously explored for encapsulation, these reports have been restricted to [water-in-oil]-in-oil systems and employ stepwise solvent evaporations to harden a polymer shell around the desired core. In our work, we challenge this approach by employing the multiple-phase concept to encapsulate ILs and leverage shell-forming precursors loaded into the interphase for thiol-ene crosslinking to give microcapsule shell, thus overcoming tedious optimization of solvent removal. Gravimetric sorption-desorption experiments demonstrate that this microencapsulation template significantly increased the uptake rate of CO2 compared to the bulk IL and that the microcapsules are stable to CO2 uptake and thermal release cycles. In all, this novel strategy offers researchers across materials science and engineering a creative approach to microencapsulation of viscous fluids and harnesses previously unexplored shell-forming precursors, thus expanding the scope beyond those commonly reported in the literature (specifically polymer shells derived from A2-B2 interfacial polymerizations).

CO<sub>2</sub> solubility in ILs results from the poor packing of ions in the liquid (i.e., high free volume), with capacity impacted by the pairing of cation and anion. 16-18 Enhanced CO2 solubility is generally observed with ions containing fluoroalkyl groups, 19 as well as integration of amine functionalities which allow for chemisorption in addition to physisorption. 20-23 However, many applications involving ILs are limited by slow mass transfer rates due to high viscosities.<sup>24</sup> This challenge is often resolved by increasing the accessible IL surface area via physical agitation25 or by microencapsulation.26 In comparison to their bulk IL counterparts, microencapsulated ILs exhibit enhanced performance in gas uptake with the added benefit of being handled as a sorbent for packed bed separations.<sup>27</sup>

Common techniques for microencapsulation include microfluidics, the hard-template approach, and the soft-template method. Microfluidic techniques offer excellent control over microcapsule diameter, commonly in the range of 1-500 microns, and shell thickness. Zhao et al., for instance, reported a capillary microfluidic system to prepare monodisperse polymeric

<sup>&</sup>lt;sup>a</sup> Dept. of Chemistry, Texas A&M University, College Station, TX 77843, USA. E-mail: emilypentzer@tamu.edu

<sup>&</sup>lt;sup>b</sup> Dept. of Materials Science & Engineering, Texas A&M University, College Station, TX 77843. USA

<sup>&</sup>lt;sup>c</sup> Dept. of Chemical and Biomolecular Engineering, Case Western Reserve University, Cleveland, OH 44106, USA

<sup>†</sup> Electronic supplementary information (ESI) available. See DOI: https://doi.org/

Communication

microcapsules loaded with CO<sub>2</sub> solvents or chelating agents.<sup>28</sup> Notably, however, this approach has the stringent requirement that monomers are immiscible in both the droplet and continuous phases, and is difficult for highly viscous liquids, such as ILs.<sup>29</sup> Alternatively, *via* the hard-template approach, a shell is first grown atop a sacrificial template (e.g., silica particle);<sup>30,31</sup> the rigid template is then removed and the hollow shell is backfilled with the desired liquid core. For example, Moya et al. encapsulated the IL trihexyl(tetradecyl)-phosphonium 2-cyanopyrrolide ([P<sub>66614</sub>][2-CNPyr]) in a porous carbon shell; the resulting capsules preserved the CO2 uptake capabilities of the IL and demonstrated enhanced CO<sub>2</sub> adsorption rates compared to the bulk.<sup>32</sup> However, the hardtemplate approach is limited by time-consuming multistep processes and the use of harsh reagents (e.g., hydrofluoric acid). Perhaps more widely utilized, soft-template microencapsulation generally leverages emulsion-based interfacial polymerization between a multifunctional monomer in the continuous phase and a complementary monomer in the discontinuous phase.<sup>33</sup> Our group and others have reported the use of interfacial poly-

merization in Pickering emulsions, those stabilized by solid

particles, to produce microcapsules with an IL core for various

applications.34-37 Recently, Al-Mahbobi et al. encapsulated IL/

amine mixtures by coupling hydrophobized graphene oxide

nanosheets as particle surfactants with diamine/diisocyanate

monomers, demonstrating the encapsulated formulation's utility

in mitigating the evaporation of volatile small molecule amines

and increasing the adsorption rate of CO2.38 In the soft-template

approach, the reliance on interfacial polymerization leads to

contamination of the core liquid with monomer which may, for

example, impact properties and alter performance, thus necessi-

tating complimentary approaches to microencapsulation. A double emulsion soft-template offers an attractive alternative to its single emulsion counterpart due to the presence of multiple internal phases which can be harnessed for microencapsulation. For example, Viswanathan  $et\ al.$  reported the use of a [water-in-oil<sub>1</sub>]-in-oil<sub>2</sub> (W/O<sub>1</sub>/O<sub>2</sub>) emulsion to prepare non-porous protein microspheres with high entrapment efficiency ( $\sim$ 70%). The authors first prepared an aqueous protein-in-DCM/MeCN emulsion under high shear in the presence of a polymeric surfactant. An aliquot of this single emulsion was added to liquid paraffin

containing an additional surfactant and low shear emulsification resulted in formation of the  $W/O_1/O_2$  emulsion. Extraction of DCM from the  $O_1$  into the paraffin  $O_2$ , then slow evaporation of MeCN from  $O_1$ , resulted in polymer precipitation and hardening around a core of an aqueous protein solution, thus yielding microspheres with a polymer shell. Critically, the double emulsion template provides an interphasial region (e.g.,  $O_1$ ) between the innermost droplet (W) and outermost continuous phase  $(O_2)$  which could be used for shell-forming chemistry without the need for reagents in the inner aqueous (W) phase, thereby preserving purity of the resulting core. Although the use of double emulsions for microencapsulation holds great potential in tailoring the core and shell composition of microcapsules, these systems remain severely underdeveloped.

Herein, we report, for the first time, a microencapsulation strategy based on a non-aqueous [IL-in-oil<sub>1</sub>]-in-oil<sub>2</sub> (IL/O<sub>1</sub>/O<sub>2</sub>) double emulsion soft-template to produce microcapsules with pristine core of IL and use of these solid-liquid composites in carbon capture. The hypothesis of this work is that the mixed O<sub>1</sub> interphase can be selectively loaded with precursors for thiol-ene crosslinking, thus localizing shell-formation to the interphase and encapsulating IL droplets (Fig. 1). To this end, a CO2-derived polycarbonate bearing vinyl pendant groups was synthesized and incorporated into the O<sub>1</sub> interphase of an IL/O<sub>1</sub>/O<sub>2</sub> double emulsion, along with a multifunctional thiol crosslinker and photoinitiator. After double emulsion formation, microcapsule fabrication was driven by UV-initiated thiol-ene crosslinking in the interphase, producing core-shell structures with enhanced CO2 uptake compared to their bulk IL counterparts. This novel strategy offers researchers across materials science and engineering an innovative approach to microencapsulation of viscous fluids and harnesses previously unexplored shell-forming precursors, thus expanding the scope beyond those commonly reported in the literature (i.e., polymer shells derived from A2-B2 interfacial polymerization).

#### Results and discussion

Our soft-template approach to IL microencapsulation is based on a two-step emulsification process to prepare a double

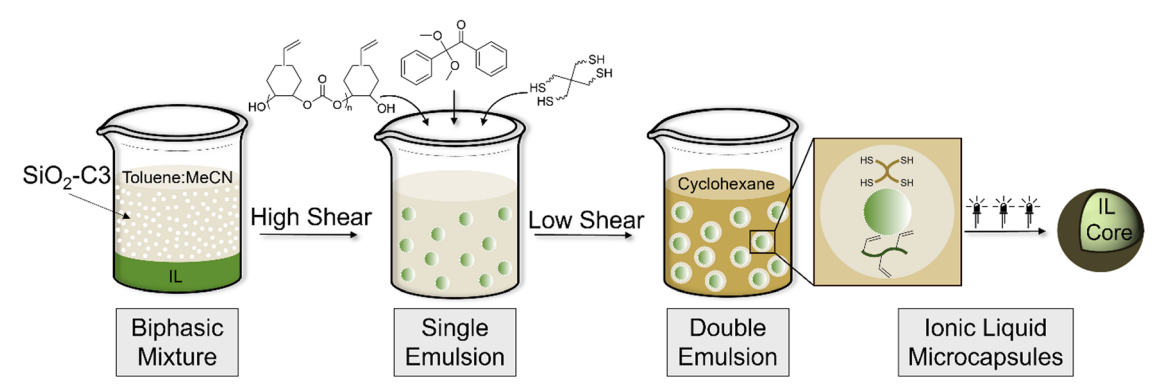


Fig. 1 Scheme depicting stepwise fabrication of IL microcapsules via thiol—ene crosslinking of a polycarbonate bearing pendant alkenes with small molecule multifunctional thiols in the  $O_1$  interphase of an [IL-in-oil<sub>2</sub>]-in-oil<sub>2</sub> (IL/ $O_1/O_2$ ) double emulsion.

Materials Horizons Communication

emulsion, followed by crosslinking of reagents in the interphase. To stabilize the IL-in-oil (IL/O<sub>1</sub>) primary emulsion, colloidal silica particles 22 nm in diameter were first functionalized with trimethoxy(propyl)silane, as previously reported;<sup>44</sup> these SiO<sub>2</sub>-C3 particles were dispersible in toluene and interfacially active at the IL/O<sub>1</sub> interface, serving as Pickering surfactants. Fourier transform infrared spectroscopy (FTIR) and thermogravimetric analysis (TGA) confirmed functionalization of the SiO2 surface, in agreement with prior reports (Fig. S3, ESI†).36 The continuous oil phase of the primary emulsion was a 4:1 toluene/MeCN mixture (O<sub>1</sub>), which was established by trial-and-error and dictated by the ability to form the desired secondary (double) emulsion. Thus, probe sonication (high shear) of a biphasic system comprised of IL ([BMIM][BF<sub>4</sub>], [BMIM][PF<sub>6</sub>], or [EMIM][BF<sub>4</sub>]) and toluene/MeCN with dispersed SiO<sub>2</sub>-C3 was used to achieve spherical droplets of IL in oil, microns in diameter, as observed under optical microscopy (Fig. 2A-C). To form the IL/O<sub>1</sub>/O<sub>2</sub> double emulsion, an aliquot of primary IL/O1 emulsion was added under low shear (600 rpm) via micropipette to the O2 solution which was a 17:2:1 mixture (by mass) of cyclohexane/toluene/Span<sup>®</sup> 85. We posit that the presence of toluene in both O1 and O2 slows the rapid extraction of toluene into cyclohexane, thus maintaining the mixed O<sub>1</sub> interphase for shell-forming chemistry. Moreover, the presence of MeCN in the primary continuous phase (O1) prevents miscibility with the secondary continuous phase (O<sub>2</sub>), allowing for double emulsion formation. IL/O<sub>1</sub>/O<sub>2</sub> double emulsion droplets were observed via optical microscopy, with the IL core highlighted in a magenta hue and the toluene/MeCN interphase indicated by the green circumference (Fig. 2D and E). Critically, the O<sub>1</sub>

interphase separates the IL from the secondary continuous phase  $(O_2)$  and serves as a site for shell formation around the IL. In the absence of Span<sup>®</sup> 85, double emulsion droplets were not stable.

To achieve IL microcapsules, a CO2-derived polycarbonate bearing vinyl pendant groups (poly(VCHO)), pentaerythritol tetrakis(3-mercaptopropionate) crosslinker (PETMP), and photoinitiator (DMPA) were added to the continuous phase of the IL/O<sub>1</sub> primary emulsion prior to double emulsion formation. The polymer was prepared using a salen Co(III)TFA/ PPNTFA binary catalyst system as we previously reported, 45 giving a polymer with an M<sub>n</sub> of 23.1 kDa and dispersity of 1.4 (Fig. S4, ESI†). Notably, both PETMP and DMPA were selectively soluble in toluene/MeCN which localizes the shell formation in the interphase of the double emulsion. The vessel containing the double emulsion was transferred to a UV photoreactor and irradiated for 20 minutes, resulting in thiol-ene crosslinking of poly(VCHO) and PETMP around the IL droplets, forming a composite shell. This transformation was marked by an apparent shift of the double emulsion from translucent (preirradiation) to opaque (post-irradiation). Further, upon irradiation the microcapsules settled at the bottom of the vessel, allowing for repeated rounds of washing with pentane and gravity settling to remove any unreacted components, prior to drying the microcapsules under reduced pressure and isolation as a solid powder. Importantly, in the absence of DMPA or UV irradiation, microcapsule formation was not observed, and the double emulsion persisted. Scanning electron microscopy (SEM) of the isolated microcapsules revealed a relatively smooth surface and non-uniform size distribution (Fig. 2G-I), as is commonly observed for microcapsules prepared via soft-template

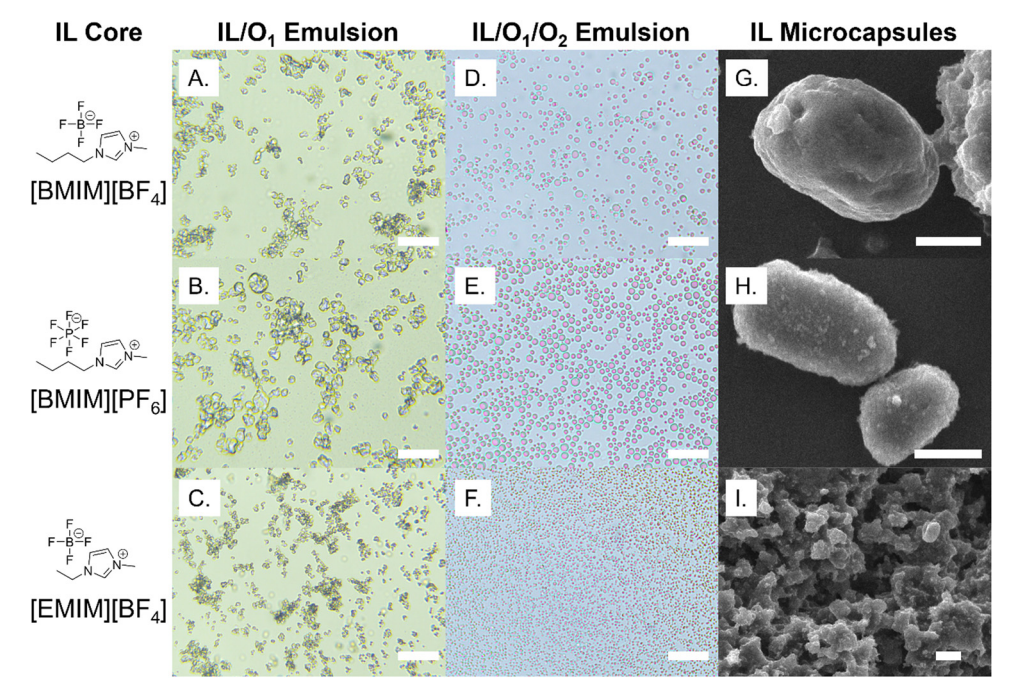


Fig. 2 Optical microscopy images of (A)–(C) IL-in-oil<sub>1</sub> (IL/O<sub>1</sub>) single emulsions stabilized by  $SiO_2$ –C3 and (D) and (E) [IL-in-oil<sub>1</sub>]-in-oil<sub>2</sub> (IL/O<sub>1</sub>/O<sub>2</sub>) double emulsions stabilized by modified silica (primary, inner interface) and Span<sup>®</sup>85 (secondary, outer interface); SEM images of (G)–(I) IL microcapsules fabricated by *via* thiol–ene crosslinking in the interphase. Scale bars for all optical microscopy images are 50  $\mu$ m; scale bars for all SEM images are 10  $\mu$ m.

methods. Microcapsule diameter was determined by laser diffraction (Table S1, ESI $\dagger$ ); on average, [BMIM][BF $_4$ ] microcapsules were approximately 15 µm in diameter, whereas [BMIM][PF $_6$ ] and [EMIM][BF $_4$ ] microcapsules were slightly larger, around 30 µm (Fig. S5, ESI $\dagger$ ).

Communication

Double emulsion-templated microcapsules were characterized by FTIR spectroscopy, TGA, and extraction of the IL core. Shown in Fig. 3A, the FTIR spectrum of neat [BMIM][BF<sub>4</sub>] shows stretching frequencies at 3161 cm<sup>-1</sup> and 3120 cm<sup>-1</sup> attributed to aromatic C-H stretching; 2961 cm<sup>-1</sup> and 2875 cm<sup>-1</sup> indicative of aliphatic C-H stretching; and 1572 cm<sup>-1</sup> and 1170 cm<sup>-1</sup> indicative of the imidazolium C-C and C-N bonds, respectively. 46-48 The FTIR spectrum of the [BMIM][BF<sub>4</sub>] microcapsules exhibits these same peaks as expected, in addition to a stretching frequency at 1735 cm<sup>-1</sup> attributed to the C=O on the polycarbonate. Notably, characteristic vinyl C=CH stretching frequencies at 3079 cm<sup>-1</sup> and 1639 cm<sup>-1</sup> are present in the spectrum of the neat poly(VCHO) (Fig. S6, ESI†), but are not observed in the spectrum of the microcapsules, indicating consumption of the vinyl groups. Microcapsule composition was further analyzed by extracting the IL core with multiple acetone washes, then characterizing the dried shell via FTIR spectroscopy. Notably, the spectrum of the shells lacks signals associated with bulk IL, suggesting complete core removal, and exhibits signals at 2928 cm<sup>-1</sup> and 2860 cm<sup>-1</sup> from polymer C-H stretching, 1735 cm<sup>-1</sup> from the C=O, and 1119 cm<sup>-1</sup> from characteristic carbonate stretching. In TGA weight loss profiles, bulk [BMIM][BF<sub>4</sub>] degrades in a single mass loss event above 400 °C, in agreement with prior reports, 49 whereas the corresponding microcapsules show mass loss around 340 °C from degradation of the [BMIM][BF4] core with approximately 15 wt% residual mass, which we attribute to the presence of silica from the single emulsion within the composite shell (Fig. 3B). This is further supported by the TGA weight loss profile of the hollow shells, which demonstrates a higher residual mass ( $\sim 30$  wt%, Fig. 3B).

SEM-EDS analysis of the dried microcapsules indicates the presence of oxygen (40.3 wt%), carbon (25.8 wt%), and sulfur (0.7 wt%) on the surface of the  $[BMIM][BF_4]$  microcapsules, which support the surface localization of the crosslinked thiolene shell. In addition, silicon (15.2 wt%) is observed, which we attribute to localization of silica-based Pickering surfactants

(SiO<sub>2</sub>-C3) within the shell. As the sampling depth of SEM-EDS is approximately 2  $\mu$ m,<sup>50</sup> fluorine (10.8 wt%) and nitrogen (7.2 wt%) from the [BMIM][BF<sub>4</sub>] core are also detected. Thus, some IL may be within (*e.g.*, plasticizing) the polymer shell (Fig. 3C).

The loading of IL in the [BMIM][BF4] microcapsules was established by determining core weight percent via extraction of the IL into deuterated dimethoxy sulfoxide (DMSO-d6) containing approximately 0.050 M of mesitylene as an internal standard and characterization by <sup>1</sup>H NMR spectroscopy (Fig. S2, ESI†). The loading of [BMIM][BF4] was found to be  $62.0 \pm 0.5$  wt% across three trials, suggesting that approximately 36% of the microcapsules by mass is the composite shell (Table S2, ESI†). To demonstrate the modularity of this double emulsion soft-template platform, we also microencapsulated [BMIM][PF<sub>6</sub>] and [EMIM][BF<sub>4</sub>], obtaining core loading values of  $62.8 \pm 0.6$  wt% and  $61.3 \pm 0.3$  wt%, respectively. FTIR analysis of [BMIM][PF<sub>6</sub>] and [EMIM][BF<sub>4</sub>] microcapsules supports both the presence of the IL as well as the crosslinked polycarbonate (Fig. S7, ESI $\dagger$ ), consistent with the results of the [BMIM][BF<sub>4</sub>] microcapsules discussed above. Additionally, TGA weight loss profiles for the microencapsulated ILs show reasonable correlation to the bulk, as expected (Fig. S8, ESI†).

Encapsuled ILs have recently emerged as promising constructs for carbon capture and thus we assessed the CO2 uptake and release performance of the microcapsules prepared from double emulsions, comparing to the corresponding bulk IL (Fig. 4). A small sample of microcapsules or bulk IL was loaded onto a TGA pan; CO<sub>2</sub> uptake was performed at 30 °C for 30 min, followed by desorption under N2 for 10 min. An initial sorption-desorption cycle was performed to condition the samples (Fig. S9, ESI†) and the performance of the hollow shell was also evaluated to determine the shell contribution to the uptake capacity (Fig. S10, ESI†). Fig. 4 shows the gravimetric CO<sub>2</sub> uptake and release of the three types of IL microcapsules, with the performance of the bulk IL shown in dashed lines and that of the microcapsules in the solid lines; normalized capacities are tabulated respective to wt% of IL in each microcapsule to determine the performance of the encapsulated IL (Table 1). Furthermore, CO<sub>2</sub> sorption isotherms of microcapsules were also obtained at 30 °C in the pressure range of 0-1 bar, similar to the previously reported procedure, 51 as shown in Fig. 4D.

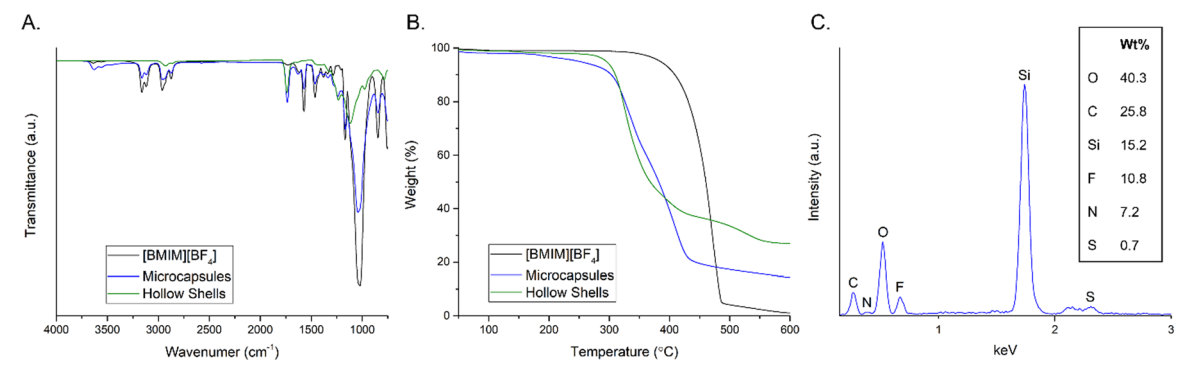


Fig. 3 FTIR spectra (A) and TGA weight loss profiles (B) for bulk [BMIM][BF<sub>4</sub>] (black traces), IL microcapsules (blue traces), and hollow shells (green traces); EDS spectrum (C) for [BMIM][BF<sub>4</sub>] microcapsules.

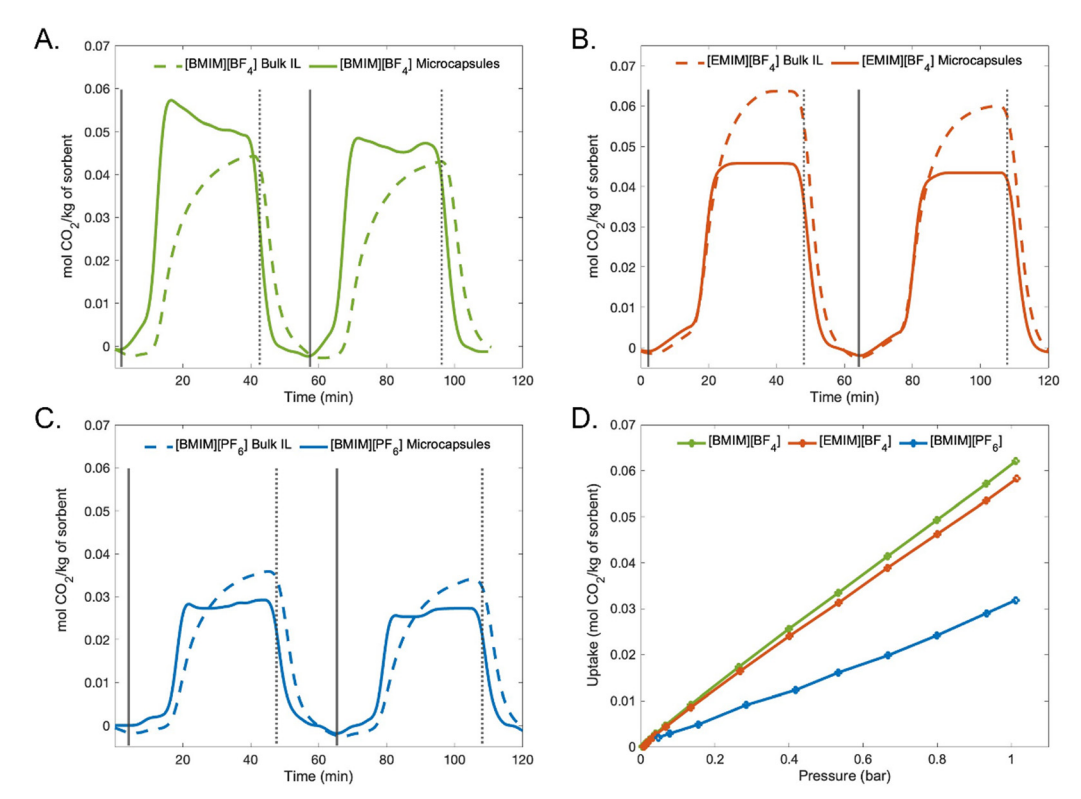


Fig. 4 Gravimetric CO<sub>2</sub> sorption (30 °C, 1 bar) and desorption (65 °C, 1 bar) for bulk IL and microcapsules of (A) [BMIM][BF<sub>4</sub>], (B) [EMIM][BF<sub>4</sub>], and (C) [BMIM][PF<sub>6</sub>]; (D) CO<sub>2</sub> volumetric isotherms of [BMIM][BF<sub>4</sub>], [EMIM][BF<sub>4</sub>], and [BMIM][PF<sub>6</sub>] microcapsules at 30 °C. Vertical solid lines represent sorption of pure CO<sub>2</sub>; vertical dashed lines represent desorption under N<sub>2</sub>.

Overall, these CO<sub>2</sub> capacities are comparable to those obtained by TGA at 30 °C and 1 bar. We also note that the CO<sub>2</sub> uptake increased linearly as the partial pressure of CO2 increased, demonstrating the characteristic behavior of physisorption. Notably, [BMIM][BF4] microcapsules demonstrated the highest overall CO<sub>2</sub> uptake (0.06 mol kg<sup>-1</sup> sorbent) as compared to [EMIM][BF<sub>4</sub>] and [BMIM][PF6] microcapsules. While the demonstrated CO2 solubilities are not necessarily significant in comparison to the more recent functionalized ILs demonstrated for low partial pressures, the utility of the demonstrated microcapsules can be envisioned for separations under moderate CO<sub>2</sub> pressures where physisorption capacity increases linearly with pressure.

The microcapsules prepared from the double emulsion could readily be used for carbon capture with packed beds, as opposed to transport-limited gas uptake by the viscous bulk ILs. Table 1 summarizes the performance of the [BMIM][BF<sub>4</sub>] microcapsules with the CO<sub>2</sub> capacity normalized to both the starting weight of each cycle and the wt% IL, as well as capacity of the hollow shells; these data were collected for 30 minutes of CO<sub>2</sub> sorption, enough time for all samples to reach a stable weight, at which capacity was determined. For bulk [BMIM][BF<sub>4</sub>], the CO<sub>2</sub> capacity is 0.046 and 0.045 mol CO<sub>2</sub> per kg for the first and second cycle, respectively (i.e., after conditioning). Normalized to the wt% of the bulk IL in the microcapsules, the expected

Table 1 Normalized capacities of microcapsule components and saturation percent of microcapsules

IL			$[BMIM][BF_4]$	$[EMIM][BF_4]$	[BMIM][PF <sub>6</sub> ]
IL wt% in microcapsules		Cycle #	$62.0 \pm 0.5\%$	$61.3 \pm 0.3\%$	$62.8 \pm 0.6\%$
Normalized capacity (mol CO <sub>2</sub> per kg of sorbent)	Bulk IL	1st	0.028	0.039	0.023
		2nd	0.028	0.039	0.023
	Hollow shell	1st	0.028	0.027	0.023
		2nd	0.028	0.027	0.023
	Microcapsules	1st	0.050	0.047	0.029
		2nd	0.050	0.046	0.030
Saturation% of CO <sub>2</sub> in core IL		1st	90	70	62
		2nd	89	70	65
Sorption rate (mmol CO <sub>2</sub> per min)	Bulk IL	1st	7.0	12.3	7.1
		2nd	<b>5.</b> 7	11.6	6.4
	Microcapsules	1st	31.2	33.4	13.0
	_	2nd	29.7	35.4	11.3

capacity is 0.028 CO<sub>2</sub> per kg (Table 1); the IL-normalized capacities for the microcapsules are 0.050 and 0.050 mol CO<sub>2</sub> per kg for the first and second cycle, respectively. The capacity for the microcapsules is consistent with the value of the combined capacity of the IL and shell (sum of values measured independently). For example, the uptake of the hollow shell in the first cycle is 0.028 mol CO<sub>2</sub> per kg, and that of the bulk [BMIM][BF<sub>4</sub>] is 0.028 mol CO<sub>2</sub> per kg as well, giving a summation of 0.056 mol CO<sub>2</sub> per kg; as the capacity of the [BMIM][BF<sub>4</sub>] microcapsules is 0.053 mol CO<sub>2</sub> per kg, the microcapsules reach 90% of the expected value (Table 1). The analyses of [EMIM][BF<sub>2</sub>] and [BMIM][BF<sub>3</sub>] are

Communication

example, the uptake of the hollow shell in the first cycle is 0.028 mol CO<sub>2</sub> per kg, and that of the bulk [BMIM][BF<sub>4</sub>] is 0.028 mol CO<sub>2</sub> per kg as well, giving a summation of 0.056 mol CO<sub>2</sub> per kg; as the capacity of the [BMIM][BF<sub>4</sub>] microcapsules is 0.053 mol CO<sub>2</sub> per kg, the microcapsules reach 90% of the expected value (Table 1). The analyses of [EMIM][BF<sub>4</sub>] and [BMIM][PF<sub>6</sub>] are summarized in Table 1 and reveal that the microcapsules have  $\sim$  70% and 62% CO<sub>2</sub> capacity relative to the summation of the components; these lower saturation values may be attributed to the larger size of these microcapsules and longer pathway of diffusion of CO2 to the inner liquid core. Table S3 (ESI†) summarizes the performance of these microcapsules compared to literature CO<sub>2</sub> capacities of encapsulated ILs. At similar conditions, the capacities seem to differ as large as an order of magnitude based on the encapsulation method and the shell material. This emphasizes the impact shell material and method of preparation, in addition to core wt% loading and microcapsule size, on the performance of encapsulated ILs in CO2 capture. The results reported herein help bridge the gaps in the literature to better understand

factors that affect the behavior of ENILs in CO2 uptake.

In complement to considerations of the capacity of solid-liquid hybrids in carbon capture, the time to saturation can also be considered, as the increased surface area afforded by the microcapsules may increase sorption rate. For the microcapsules and bulk IL, the uptake rate was calculated as the slope of the initial linear portion of sorption curves. As summarized in Table 1, the sorption rates for the bulk liquids in the first cycle were 7.0, 12.3, and 7.1 mmol CO<sub>2</sub> per min for [BMIM][BF<sub>4</sub>], [EMIM][BF<sub>4</sub>], and [BMIM][PF<sub>6</sub>], respectively. In contrast, the [BMIM][BF<sub>4</sub>], [EMIM][BF<sub>4</sub>], and [BMIM][PF<sub>6</sub>] microcapsules demonstrate a much higher rate of 31.2, 33.4, and 13.0 mol CO<sub>2</sub> per min, respectively (i.e., 2-4 times faster). Similar trends are observed for the second cycle as well. Notably, the shape of the sorption curve for the microcapsules indicates rapid uptake followed by an immediate decrease in capacity before plateauing; this may be due to shell expansion or swelling during CO<sub>2</sub> uptake cycles, which would cause a change in density. Thus, the uptake rates are improved for all three types of microcapsules; this may be somewhat surprising if the shell is considered a physical barrier and supports that the shell is permeable to CO2. These results support that IL microencapsulation from double emulsions can be used to tailor CO<sub>2</sub> capture performance, mitigating diffusion limitation associated with higher viscosities of ILs by increasing the contact surface area, and further demonstrates the applicability of this approach to other ILs and task-specific ILs (TSILs) that face diffusion limitations.

#### Conclusions

Herein we report a novel microencapsulation strategy for ILs using an  $IL/O_1/O_2$  double emulsion as a soft-template.

The IL/O<sub>1</sub>/O<sub>2</sub> system was prepared such that the mixed-oil interphase (O<sub>1</sub>), situated between the IL droplet core and outermost continuous phase (O2), could be loaded with precursors for on-demand microcapsule shell fabrication around the inner IL droplet. To this end, a CO2-derived polycarbonate bearing vinyl pendant groups was synthesized and added to the interphase, along with a tetrathiol crosslinker and photoinitiator, both of which demonstrate selective solubility for the interphase. UV irradiation of the double emulsion resulted in thiol-ene crosslinking of the polycarbonate, forming a robust shell around the IL droplets without the need for monomer addition to the core, thus preserving purity of the microencapsulated fluid. Gravimetric sorption-desorption experiments demonstrate that this microencapsulation template significantly increased the uptake rate of CO<sub>2</sub> compared to the bulk IL and that the microcapsules were stable to cycles of CO2 uptake and thermal release. This work demonstrates a distinctly new approach to enhancing the performance of viscous ILs and other liquids tailored for carbon capture and provides opportunities to modify shell thickness, permeability, and selectivity as crucial to enhanced performance at low CO2 pressures, such as direct air capture. This method also demonstrates a creative approach to recycling CO2, as it serves as an essential building block for the polymer which ultimately becomes the shell of IL microcapsules employed in CO2 capture. Ongoing work in our lab focuses on tailoring this double emulsion framework to encapsulate TSILs relevant to CO<sub>2</sub> capture, as well as tuning the shell properties for complimentary applications.

#### Author contributions

NS, ECB, and EP conceived the research. NS performed all experiments and prepared the original manuscript. LA collected TGA measurements and performed data analysis. MZ performed volumetric  ${\rm CO_2}$  sorption experiments. EP and BG acquired funding. All authors reviewed and edited the manuscript.

## Data availability

The data supporting this article has been included as part of the ESI. $\dagger$ 

#### Conflicts of interest

There are no conflicts to declare.

## Acknowledgements

Use of the TAMU Materials Characterization Core Facility (RRID:SCR\_022202), TAMU Soft Matter Facility (RRID:SCR\_022482), and TAMU Microscopy & Imaging Center (RRID:SCR\_022128) is acknowledged. The authors thank Dr. James Batteas (TAMU Dept. of Chemistry) for gracious use of his lab's FTIR spectrometer. N. S. is supported by an NSF Graduate Research Fellowship (Award #2139772). E. P. thanks NSF DMR grant #2103182 and U.S. DOE award #DE-SC0022214.

# Materials Horizons References

- 1 Z. Lei, B. Chen, Y.-M. Koo and D. R. MacFarlane, *Chem. Rev.*, 2017, **117**, 6633–6635.
- 2 G. Kaur, H. Kumar and M. Singla, J. Mol. Liq., 2022, 351, 118556.
- 3 R. L. Vekariya, J. Mol. Liq., 2017, 227, 44-60.
- 4 O. Zech, A. Stoppa, R. Buchner and W. Kunz, *J. Chem. Eng. Data*, 2010, 55, 1774–1778.
- 5 A. K. Verma, A. S. Thorat and J. K. Shah, *J. Ionic Liq.*, 2024, 4, 100089.
- 6 C. Maton, N. De Vos and C. V. Stevens, *Chem. Soc. Rev.*, 2013, 42, 5963.
- 7 B. Wang, L. Qin, T. Mu, Z. Xue and G. Gao, *Chem. Rev.*, 2017, **117**, 7113–7131.
- 8 M. Ahrenberg, M. Beck, C. Neise, O. Keßler, U. Kragl, S. P. Verevkin and C. Schick, *Phys. Chem. Chem. Phys.*, 2016, **18**, 21381–21390.
- 9 O. Aschenbrenner, S. Supasitmongkol, M. Taylor and P. Styring, *Green Chem.*, 2009, 11, 1217.
- 10 Q. Liu, C. Gui, G. Li and Z. Lei, *ACS Sustainable Chem. Eng.*, 2023, **11**, 7573–7585.
- 11 T. Sukhbaatar, S. Dourdain, R. Turgis, J. Rey, G. Arrachart and S. Pellet-Rostaing, *Chem. Commun.*, 2015, **51**, 15960–15963.
- 12 X. Han and D. W. Armstrong, Acc. Chem. Res., 2007, 40, 1079-1086.
- 13 S. P. M. Ventura, F. A. E. Silva, M. V. Quental, D. Mondal, M. G. Freire and J. A. P. Coutinho, *Chem. Rev.*, 2017, 117, 6984–7052.
- 14 W. Faisal Elmobarak, F. Almomani, M. Tawalbeh, A. Al-Othman, R. Martis and K. Rasool, *Fuel*, 2023, 344, 128102.
- 15 S. K. Shukla, S. G. Khokarale, T. Q. Bui and J.-P. T. Mikkola, *Front. Mater.*, 2019, **6**, 42.
- 16 P. Husson-Borg, V. Majer and M. F. Costa Gomes, J. Chem. Eng. Data, 2003, 48, 480–485.
- 17 C. Cadena, J. L. Anthony, J. K. Shah, T. I. Morrow, J. F. Brennecke and E. J. Maginn, *J. Am. Chem. Soc.*, 2004, 126, 5300–5308.
- 18 M. B. Shiflett and A. Yokozeki, *Ind. Eng. Chem. Res.*, 2005, **44**, 4453–4464.
- 19 M. J. Muldoon, S. N. V. K. Aki, J. L. Anderson, J. K. Dixon and J. F. Brennecke, *J. Phys. Chem. B*, 2007, **111**, 9001–9009.
- 20 B. E. Gurkan, J. C. De La Fuente, E. M. Mindrup, L. E. Ficke, B. F. Goodrich, E. A. Price, W. F. Schneider and J. F. Brennecke, J. Am. Chem. Soc., 2010, 132, 2116–2117.
- 21 A. Li, Z. Tian, T. Yan, D. Jiang and S. Dai, *J. Phys. Chem. B*, 2014, **118**, 14880–14887.
- 22 G. Cui, J. Wang and S. Zhang, *Chem. Soc. Rev.*, 2016, 45, 4307–4339.
- 23 A. N. Keller, C. L. Bentley, O. Morales-Collazo and J. F. Brennecke, *J. Chem. Eng. Data*, 2022, **67**, 375–384.
- 24 A. Giaccherini, M. Al Khatib, S. Cinotti, E. Piciollo, E. Berretti, P. Giusti, M. Innocenti, G. Montegrossi and A. Lavacchi, Sci. Rep., 2020, 10, 13433.
- 25 Q. Huang, Q. Luo, Y. Wang, E. Pentzer and B. Gurkan, *Ind. Eng. Chem. Res.*, 2019, **58**, 10503–10509.

- 26 J. Yan and F. Mangolini, RSC Adv., 2021, 11, 36273-36288.
- 27 Q. Luo and E. Pentzer, ACS Appl. Mater. Interfaces, 2020, 12, 5169–5176.
- 28 Y. Zhao, S. Moshtaghibana, T. Zhu, K. A. Fayemiwo, A. Price and G. T. Vladisavljević, J. Polym. Sci., 2022, 60, 1727–1740.
- 29 J. Li, J. Lindley-Start, A. Porch and D. Barrow, *Sci. Rep.*, 2017, 7, 6302.
- 30 Y. Zhang, B. Y. W. Hsu, C. Ren, X. Li and J. Wang, *Chem. Soc. Rev.*, 2015, **44**, 315–335.
- 31 Y. Chen, H.-R. Chen and J.-L. Shi, *Acc. Chem. Res.*, 2014, 47, 125–137.
- 32 C. Moya, N. Alonso-Morales, J. De Riva, O. Morales-Collazo, J. F. Brennecke and J. Palomar, *J. Phys. Chem. B*, 2018, **122**, 2616–2626.
- 33 X. Wang, A.-C. Amason, R. T. Miceli, P. He, Y. Lei, R. Gabbard, J. A. Wieland, R. J. Linhardt, D. T. Corr and R. A. Gross, *Colloids Surf.*, A, 2022, 648, 129243.
- 34 S. S. Gaur, K. J. Edgehouse, A. Klemm, P. Wei, B. Gurkan and E. B. Pentzer, *J. Polym. Sci.*, 2021, 59, 2980–2989.
- 35 K. R. Baca, A. N. Harders, N. Starvaggi, A. D. Yancey, Y. Wang, E. Pentzer and M. B. Shiflett, *Ind. Eng. Chem. Res.*, 2023, **62**, 14522–14536.
- 36 N. C. Starvaggi, B. J. Bradford, C. D. L. Taylor and E. B. Pentzer, *Soft Matter*, 2023, 19, 7635–7643.
- 37 C. D. L. Taylor, A. Klemm, L. Al-Mahbobi, B. J. Bradford, B. Gurkan and E. B. Pentzer, *ACS Sustainable Chem. Eng.*, 2024, acssuschemeng.4c01265.
- 38 L. Al-Mahbobi, A. Klemm, C. Taylor, B. Gurkan and E. Pentzer, ACS Appl. Eng. Mater., 2024, acsaenm.4c00118.
- 39 E. Tenorio-Garcia, A. Araiza-Calahorra, E. Simone and A. Sarkar, *Food Hydrocolloids*, 2022, **128**, 107601.
- 40 M. Iqbal, N. Zafar, H. Fessi and A. Elaissari, *Int. J. Pharm.*, 2015, **496**, 173–190.
- 41 F. Heidari, S. M. Jafari, A. M. Ziaiifar and N. Malekjani, *Adv. Colloid Interface Sci.*, 2022, **299**, 102567.
- 42 E. Pentzer, E. Cruz Barrios and N. Starvaggi, *Acc. Mater. Res.*, 2023, **4**, 641–647.
- 43 N. B. Viswanathan, P. A. Thomas, J. K. Pandit, M. G. Kulkarni and R. A. Mashelkar, *J. Controlled Release*, 1999, **58**, 9–20.
- 44 A. Schoth, K. Landfester and R. Muñoz-Espí, *Langmuir*, 2015, 31, 3784–3788.
- 45 P. Wei, G. A. Bhat, C. E. Cipriani, H. Mohammad, K. Schoonover, E. B. Pentzer and D. J. Darensbourg, *Angew. Chem., Int. Ed.*, 2022, **61**, e202208355.
- 46 J. Ren, J. Li, L. Lv and J. Wang, Environ. Sci. Pollut. Res., 2021, 28, 12909–12917.
- 47 J. Wu, M.-J. Wang and J. P. W. Stark, *J. Quant. Spectrosc. Radiat. Transfer*, 2006, **102**, 228-235.
- 48 N. Nanbu, Y. Sasaki and F. Kitamura, *Electrochem. Commun.*, 2003, 5, 383–387.
- 49 H. M. Polat, S. Kavak, H. Kulak, A. Uzun and S. Keskin, *Chem. Eng. J.*, 2020, **394**, 124916.
- 50 T. Roodbar Shojaei, S. Soltani and M. Derakhshani, *Fundamentals of Bionanomaterials*, Elsevier, 2022, pp. 139–174.
- 51 Q. Huang, Q. Luo, Y. Wang, E. Pentzer and B. Gurkan, *Ind. Eng. Chem. Res.*, 2019, **58**, 10503–10509.